Engineering Structures 179 (2019) 106–119

Contents lists available at ScienceDirect

Engineering Structures

journal homepage: www.elsevier.com/locate/engstruct

Shake table test on transverse steel damper seismic system for long span cable-stayed bridges

Lianxu Zhou[a], Xiaowei Wang[a,b], Aijun Ye[a,*]

[a] State Key Laboratory of Disaster Reduction in Civil Engineering, Tongji University, Shanghai 200092, China
[b] Department of Civil Engineering, Hohai University, Nanjing 210098, China

ARTICLE INFO

Keywords:
Shake table test
Transverse steel damper seismic system
Cable-stayed bridges
Seismic isolation
Energy dissipation
Seismic performance

ABSTRACT

In current transverse seismic design of long span cable-stayed bridges, the conventional transverse fixed system (TFS) is usually adopted. This strategy inevitably increases seismic demands of substructures and towers, leading to high seismic-induced damage risks to the bridges. To address this issue, the authors recently developed a novel Transverse Steel Damper (TSD) and correspondingly proposed an innovative TSD seismic system (TSDSS), in which the TSDs were placed at deck-tower and/or deck-bent connections. To further verify the reliability and seismic isolation efficiency of TSDSS for long span cable-stayed bridges under near- and far-fault ground motions, a series of experiments on a 1/35-scale model of a kilometer-span cable-stayed bridge were conducted on a four-shake-table testing system. Experimental results indicate that (1) compared with the conventional TFS, the TSDSS can reduce transverse displacement and curvature demands along bent/tower columns, meanwhile limiting displacements at deck-bent/tower connections to an acceptable level in engineering practice. (2) The sensitivity of TSDSS to ground motions is obviously lower than that of the conventional TFS. The isolation efficiency of TSDSS is robust regardless under near- or far-fault ground motions; (3) Increasing the yield strength of TSDs can decrease the relative displacements at deck-bent/tower connections. In general, the TSDSS is experimentally validated to be a capable and reliable strategy for the seismic design of long span cable-stayed bridges. Additionally, the shake-table test is simulated using a finite element model, which provides good agreements with the test results.

1. Introduction

In the last three decades, a large number of cable-stayed bridges have been constructed in China. These bridges usually serve as key joints in national or local transport networks. Considering the importance of these bridges in networks and to ensure the essential post-earthquake functionality, the main structural components of cable-stayed bridges, including towers, foundations and superstructures, are required to remain elastic under design-level earthquakes with a return period of 2000 years in Chinese seismic design specifications [1,2]. However, severe damages were still detected in cable-stayed bridges during some recent strong earthquakes. For example, in 1999 Chi-Chi, Taiwan earthquake, Chi-Lu Bridge suffered severe damages in the towers [3]. Therefore, how to improve the seismic performances of cable-stayed bridges has drawn increasing attentions from both the engineering and academic community. In the longitudinal direction, a full- or semi-floating system is often applied in practice. In such a system, Fluid Viscous Dampers (FVDs) [4–7] are often installed at deck-tower connections to reduce shear and bending demands at tower bottoms and foundations, meanwhile limiting relative displacements between deck and towers to a practically acceptable level. In this manner, longitudinal seismic performances of cable-stayed bridges are generally acceptable for practice. In the transverse direction, however, rigid constraints are often adopted at deck-bent/tower connections for providing enough stiffness to carry traffic and wind loads under service conditions [8]. This is the so-called conventional Transverse Fixed System (TFS), which inevitably increases seismic demands at bents (or piers), towers and foundations. To meet the seismic design requirements, these components are always designed, in an uneconomic manner, with sufficient strength capacity to resist design-level earthquakes. In this regard, transversal isolation systems for cable-stayed bridges, especially in high seismic regions, are highly demanded.

In recent years, seismic isolation techniques provide alternative solutions to the seismic design of cable-stayed bridges in the transverse direction. Most of them uses passive energy-dissipation devices to elongate transverse periods of bridges and/or enhance the damping. A

* Corresponding author.
E-mail addresses: csuzlx@tongji.edu.cn (L. Zhou), x.wang@hhu.edu.cn (X. Wang), yeaijun@tongji.edu.cn (A. Ye).

https://doi.org/10.1016/j.engstruct.2018.10.073
Received 3 June 2018; Received in revised form 25 October 2018; Accepted 26 October 2018

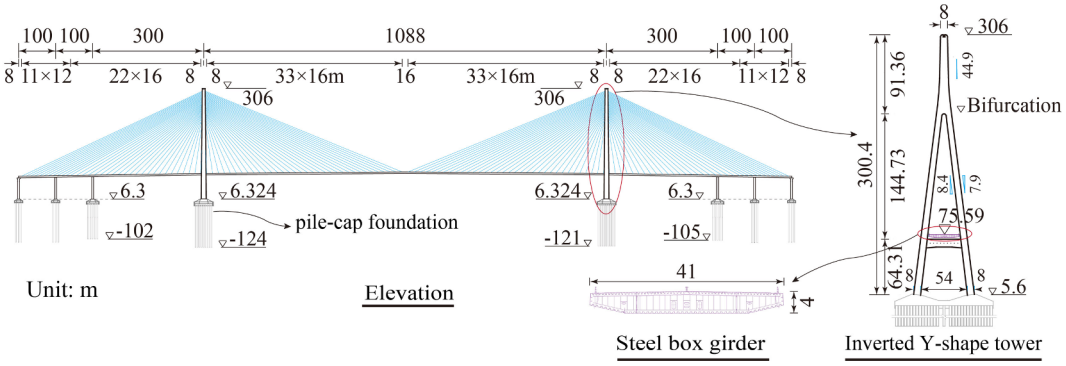

Fig. 1. Configuration of Sutong Bridge.

notable number of numerical studies have focused on the feasibility and efficiency of transverse isolation strategies for cable-stayed bridges. For example, Ye et al. [9] and Yan et al. [10] studied the effectiveness of FVDs as energy-dissipation devices installed at deck-pier connections. A noted limitation of FVDs for transverse seismic isolation is that they are difficult to adapt to deck movements in the longitudinal direction under service conditions. In other words, the transversally installed FVDs cannot readily adapt to the longitudinal full- or semi-floating system, unless with special and complex configurations [14]. To overcome this disadvantage, Shen et al. [11,12] developed a novel Transverse Steel Damper (TSD) that behaves in elastoplastic manner under earthquakes and thereby can dissipate seismic energy. In addition, it can freely adapt to the longitudinal movement of deck using simple configurations. Utilizing the TSD, Shen et al. [12] proposed a new transversal seismic system for long span cable-stayed bridges called TSD Seismic System (TSDSS). In this system, the TSDs are placed at deck-bent (or pier) connections in parallel with sliding bearings. It is worth noting that in the aforementioned studies, rigid constraints were still adopted at the deck-tower connections. To further improve the seismic performance of towers, Camara et al. [13] numerically evaluated the efficiency of FVDs and yielding Metallic Dampers (MDs) separately to reduce the tower damage. Rion-Antirion Bridge [14] in Greece applied transversal seismic protection system, comprising FVDs and fuse restraints, installed between deck and pylons to resist extreme earthquakes. Ismail et al. [15] investigated the mitigation efficiency of cable-stayed bridges with Roll-N-Cage (RNC) isolators under near-fault earthquakes. Guan et al. [16] proposed a transverse isolation system for cable-stayed bridges, in which elastic cables were placed at deck-tower connections in parallel with FVDs, and Buckling Restrained Braces (BRBs) were placed in deck-pier connections. Raheem et al. [17] presented a new concept using low yield-strength steel links as a supplemental energy dissipation system for the seismic design of cable-stayed bridges with H-shaped steel towers. However, the feasibility and reliability of the above mentioned transverse isolation systems under earthquake excitations have not been further verified by experiments.

Shake table test is a direct and reliable method to investigate the seismic behavior of structures and to verify the results of theoretical or numerical analysis. Most of the previous experiments mainly focused on the impact of non-uniform excitations on seismic responses [18–20] and the failure mechanism of cable-stayed bridges [21,22]. Relatively few researchers conducted shake-table tests to verify the efficiency and reliability of isolation system for cable-stayed bridges, especially in the transverse direction. To the knowledge of authors, existing studies limited to Xu et al. [23] and Yi et al. [24], who carried out shake table tests to demonstrate the mitigation effectiveness of C-shaped and X-shaped yield-steel dampers, respectively, used in the transverse direction of cable-stayed bridges. From the above discussions, it can be concluded that various mitigation strategies and energy-dissipation devices have been proposed and theoretically verified using numerical analyses, but the feasibility and efficiency of these devices used in cable-stayed bridges have not been well documented by experimental studies.

Using advanced shake-table facility, this study aims to verify the efficiency and reliability of TSDSS for transverse seismic mitigation of long span cable-stayed bridges. To this end, a 1/35-scale model of a kilometer-span cable-stayed bridge was excited on a four-shake-table testing system in the Multi-functional Shaking Table Lab at Tongji University, Shanghai, China. Seismic behaviors of the TSDSS and TFS under near- and far-fault ground motions were investigated and compared in terms of force, displacement and curvature demands as well as energy dissipations. For the TSDSS, the TSDs were placed at deck-bent connections in parallel with Sliding Spherical Steel Bearings (SSSB), and TSDs were installed at deck-tower connections. Additionally, the impact of TSD yield strength on seismic behavior of TSDSS was also experimentally investigated. Finally, the shake-table test is simulated using a finite element model.

2. Bridge model

2.1. Bridge prototype

The Sutong Bridge, a typical kilometer-span cable-stayed bridge as shown in Fig. 1, was taken as the prototype. It is the longest span cable-stayed bridge in China with a main-span of 1088 m and two side-spans of 500 m (300 + 100 + 100 m). The orthotropic steel box girder, with a width of 41 m and a depth of 4 m, is supported by two inclined semi-fan cable-planes radiating from the top of the 300 m-height reinforced concrete twin towers with inverted Y-shape. In the longitudinal direction, a full-floating system is adopted and FVDs are placed at deck-tower connections to limit deck displacement demands under earthquakes. In the transverse direction, for providing enough stiffness to carry traffic and wind loads under service conditions, transversely fixed bearings and wind-resistant bearings are installed at the deck-pier and deck-tower connections, respectively, namely, the conventional TFS is utilized transversally in the as-built bridge. Other information about the bridge can be found in Ref. [25].

2.2. Scale model design and instrument arrangement

A 1/35-scale model of the Sutong Bridge as illustrated in Fig. 2 was designed for the shake table test. Considering the feasibility and to ensure the quality of construction, micro concrete was used to substitute the prototype concrete, and the similarity factor of Young's modulus for concrete was designed as 0.3. The similarity factor of acceleration and gravity acceleration was 1.0. Other scale factors, as shown in Table 1, can be derived according to the similarity law [26,27].

Since this study aims to verify the efficiency and reliability of the TSDSS for cable-stayed bridges, for better experimental feasibility, some simplifications were performed as follows. (1) The cables were

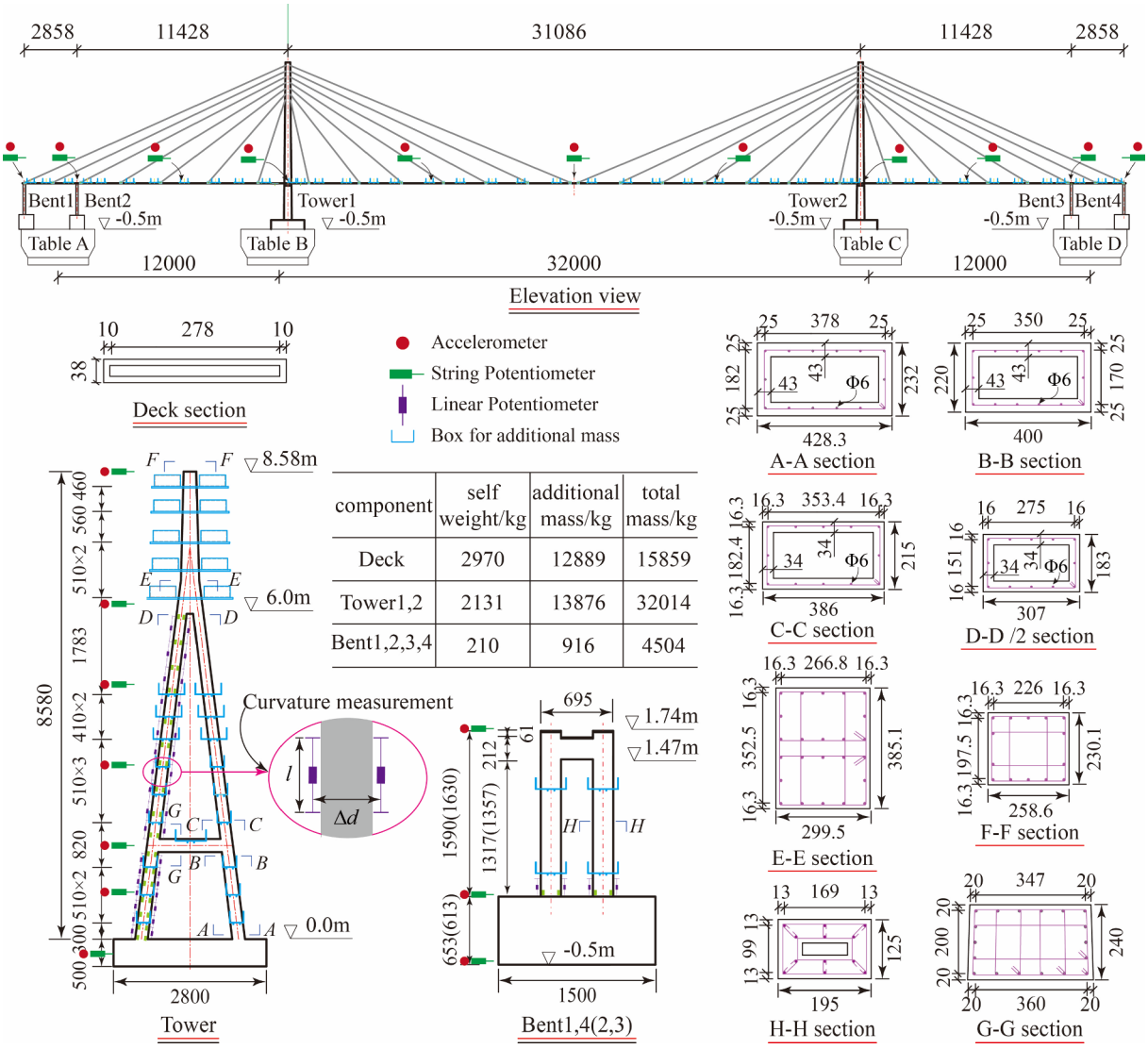

component	self weight/kg	additional mass/kg	total mass/kg
Deck	2970	12889	15859
Tower1,2	2131	13876	32014
Bent1,2,3,4	210	916	4504

Fig. 2. Details of scale model (unit: mm).

Table 1
Main scale factors for test model.

Physical quantity	Similarity relationship	Value
Length	S_l	1/35
Acceleration	$S_a = S_l/S_t^2$	1
Elastic modulus	S_E	0.3
Mass density	$S_\rho = S_E/S_a S_l$	10.5
Mass	$S_m = S_\rho S_l^3$	0.000245
Time	$S_t = (S_m/S_k)^{0.5}$	0.169
Force	$S_F = S_E S_l^2$	0.000245

reduced to 56 pairs from 272 pairs in the prototype according to the similarity of the first three order dynamic characteristics of the bridge and the forces in cables [23]. Each cable in the test model was represented by the 7.7-mm-diameter steel wire rope. (2) Soil-structure interaction effects are neglected for simplicity. (3) Due to the limited numbers of shake tables, the three piers at each side-span of the prototype bridge were condensed to two bents, which then could be mounted on one table. Under such simplifications, as shown in Fig. 2, the Bent 1 and Bent 2 were mounted on Table A, and Bent 3 and Bent 4 were mounted on Table D. Tower 1 and Tower 2 were mounted on Table B and Table C, respectively. It is worth noting that another purpose of this experiment is to investigate the lateral failure mechanism of cable-stayed bridges, which is beyond the scope of this study.

Fig. 2 also presents configurations of the scale model. The total height of the tower is 8.58 m. The total length of the deck is 59.66 m. According to the similarity of cross-sectional shear and bending capacities, section dimensions and reinforcements for towers and bents were designed. Specifically, 6-mm-diameter steel bars and galvanized wires were used to represent the longitudinal bars and reinforcement stirrups, respectively. A steel box with thickness of 10 mm was designed according to the similarity of bending stiffness along strong and weak axes of the prototype deck. Additional masses, attached along deck surface, tower shafts and bent columns, were designed as displayed in Fig. 2. Fig. 3 depicts the shake-table test system of the scale model.

To monitor the seismic responses of the structure under seismic excitations, as illustrated in Fig. 2, the deck, bents and towers were instrumented with amounts of sensors. Eleven horizontal accelerometers and eleven string potentiometers were arranged along the deck. Seven horizontal accelerometers and seven string potentiometers were installed in the same vertical plane along each tower. Each bent was instrumented with three horizontal accelerometers and three string potentiometers. The axial forces in all cables were measured by axial-force sensors as shown in Fig. 3, and tri-axial-force sensors were used to

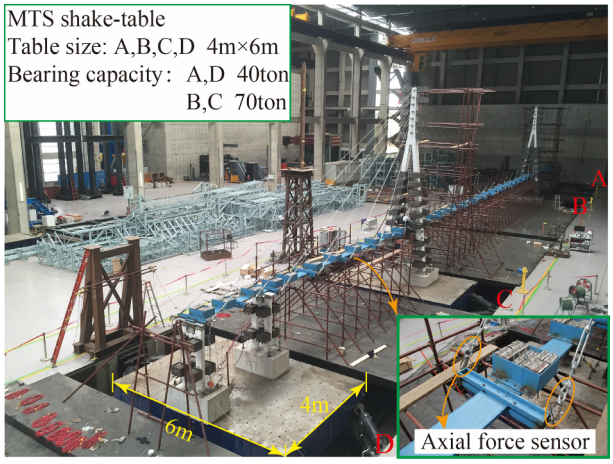

Fig. 3. Photo for full-bridge of the test model.

measure forces transferred from deck to bents and towers as shown in Fig. 5. Due to the symmetry of structure, only the forces transferred from the deck to Bent 1, Bent 2, and Tower 1 were measured. In addition, as illustrated in Fig. 2, the average section curvature along the tower column was monitored by a pair of linear potentiometers placed at two opposite faces of the tower column, which can be calculated by Eq. (1).

$$\phi = \frac{\Delta\varepsilon}{\Delta d} = \frac{\Delta h/l}{\Delta d} \tag{1}$$

where Δh is deformation difference between the two linear potentiometers; l is the vertical length of the measured region; Δd is the horizontal distance between the two potentiometers.

2.3. Description of the TSDSS and TFS

Shen et al. [11,12] recently developed a novel Transverse Steel Damper (TSD) mainly used in the transverse direction of bridges. The TSD, using triangular steel plates as the energy dissipation element, can freely accommodate the longitudinal movement of the deck under normal service conditions. The TSD possess a bilinear force-displacement property, which has been confirmed by quasi-static experiments and validated by numerical simulations [12]. Using the TSD, Shen et al. [12] proposed a novel transverse isolation system for long span cable-stayed bridges. In this system, the TSDs were placed at deck-bent (or pier) connections in parallel with sliding bearings, while fixed constraints at the transversal deck-tower connections are still applied. The sliding bearings are used to support the deck in vertical direction. Under normal service conditions, "fuse bolts" installed in the sliding bearings were used to provide transversal constraint stiffness to carry the traffic and wind loads. The designed fuse-bolts will fracture when the bridge undergoes design-level earthquakes. Consequently, the deck will be moveable in the transverse direction, meanwhile the displacement of deck will be limited to an acceptable level by TSDs.

Fig. 4 illustrates the configurations of TSDSS in this study. In each bent, one TSD is placed at the deck-bent connection in parallel with two Sliding Spherical Steel Bearings (SSSBs). In each tower, two TSDs were installed at the deck-tower connection. Fig. 5 graphically shows the prepared TSDs at the location of the Bent 2 and Tower 2. In addition, to investigate the impact of TSD yield strength on seismic behaviours of cable-stayed bridges, two types of TSDs named TSD-1 and TSD-2 were used. The system using TSD-1 is named TSDSS1, whereas the other using TSD-2 is named TSDSS2 hereinafter. The design process of TSDSS and parameters of the two types of TSDs including the mechanical and geometric parameters will be described in Section 2.4.

For comparison, the conventional TFS was also tested, in which fix constraints were applied at all deck-bent and deck-tower connections in the transverse direction. Table 2 shows the comparisons of deck-bent and deck-tower connections for the tested TSDSS1, TSDSS2 and TFS. It is worth noting again that the deck in the longitudinal direction was moveable for the three systems.

2.4. Design of the TSD

As aforementioned, TSDs were placed at deck-bent and -tower connections of the scale bridge model. With the aim of limiting displacements at deck-bent and deck-tower connections around 3 cm for

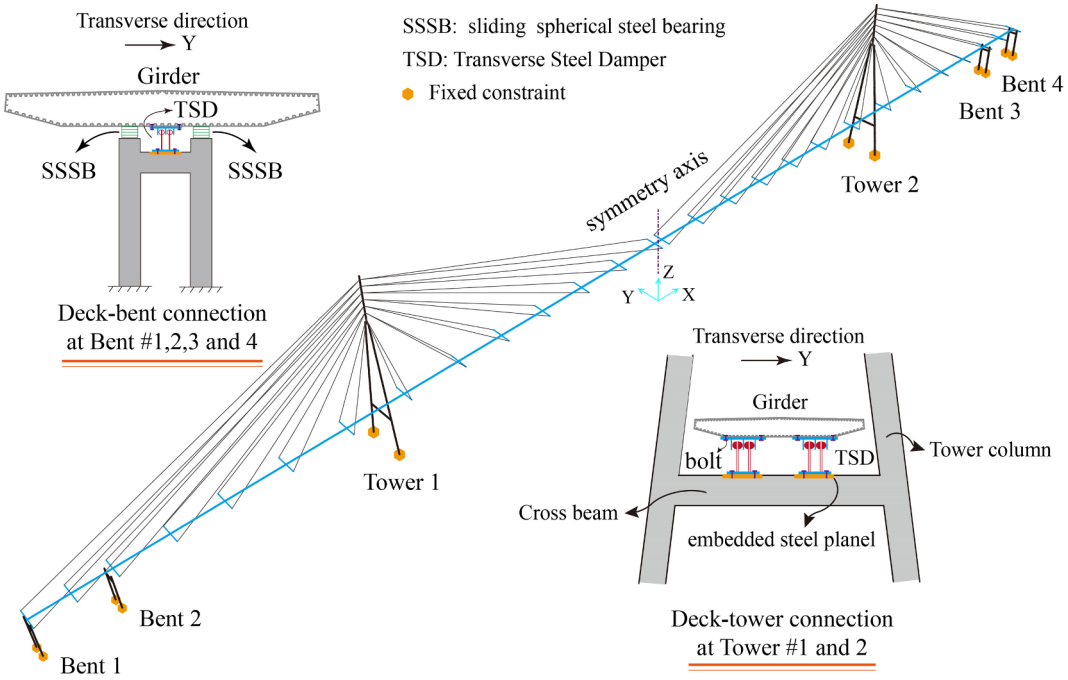

Fig. 4. Configurations of TSDSS.

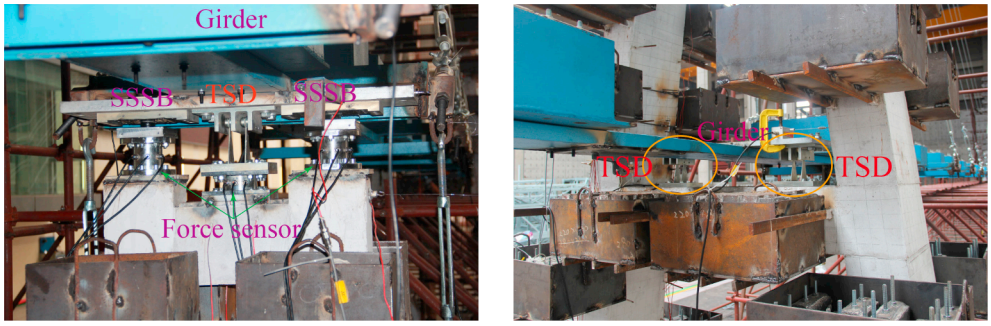

(a) Deck-bent2 connection (b) Deck-tower2 connection

Fig. 5. TSDSS photographs: TSDs installed at deck-bent/tower connections.

Table 2
Comparisons of the deck-bent/tower connections for three test models.

Direction	system	Deck-bent/tower connection	
		Bent #1, 2, 3 and 4	Tower #1 and 2
Transverse	TSDSS1	one TSD-1 + two SSSBs	two TSD-1s
	TSDSS2	one TSD-2 + two SSSBs	two TSD-2s
	TFS	Fixed	Fixed
Longitudinal	TSDSS1, TSDSS2, TFS	Moveable	Moveable

Note: SSSB = sliding spherical steel bearing.

reliable measurement purpose, these TSDs were designed using nonlinear time-history analysis in OpenSees [28]. A soft-site artificial wave (named as E10 shown in Fig. 10) that contains abundant low-frequency contents is selected as excitation, because it can trigger larger seismic demands as compared to stiff-site waves at a given intensity measure. Noted that the E10 wave is scaled to have a PGA of 0.5 g. This intensity is adopted mainly based on the following two reasons: (1) to keep the critical structural components in elastic state for testing safety and reliability. (2) within the first requirement, to trigger a large seismic demand as far as possible to reflect the effect of the TSDSS. For this purpose, a parametric analysis is then performed to determine reasonable mechanic parameters of the TSDs, including yielding force and pre- and post-yield stiffness.

More specifically, a three-dimensional finite-element-model of the scaled model with TSDs was established. In this numerical model which will be validated in Section 5, elastic beam-column elements are used to model the towers, RC bents and steel box-girder since these components are expected to remain elastic under earthquakes, and the area and inertia of gross sections shown in Fig. 2 are assigned to these elastic elements. The cables were modeled by using truss element accounting for sag effects. Nonlinear geometric effects were taken into consideration as well. The TSDs and SSSBs were simulated by zero-length spring elements with bilinear and ideal elastoplastic force-displacement

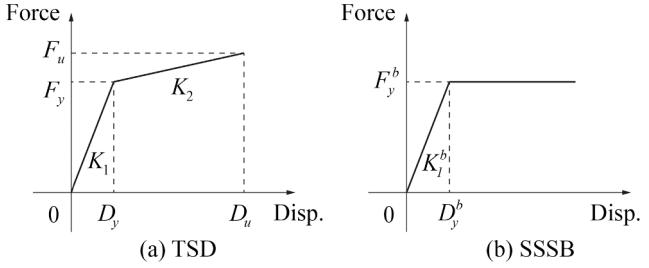

Fig. 6. Mechanical model of the TSD and SSSB.

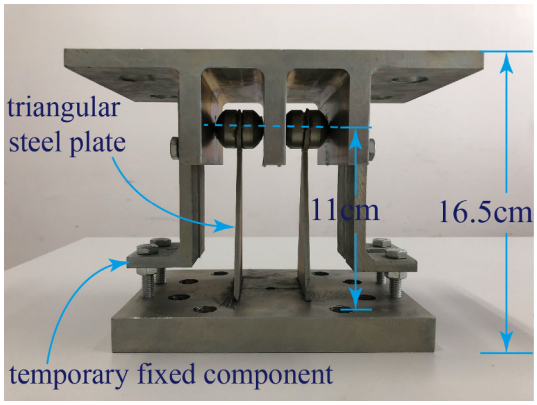

Fig. 7. Photo for the TSD.

properties, respectively, as illustrated in Fig. 6. For the SSSB, the yield strength is equal to the friction coefficient multiplied by the normal force of the bearing under dead loads. During the parametric analysis, the friction coefficient of SSSB was set as 0.02 [29–31] and the yielding displacement, D_y^b, was set as 0.002 m [1].

According to the obtained mechanical parameters of TSDs, including yield strength and pre- and post-yield stiffness, the dimensions of each triangular steel plate (i.e., width, height and thickness) and the number of plates in one TSD were designed with numerical simulation in ABAQUS [32]. Finally, as illustrated in Fig. 7, one TSD is composed of two identical triangular steel plates, each with a height of 11 cm, a width of 7 cm and a thickness of 0.3 cm. In addition, as aforementioned, two types of TSD named TSD-1 and TSD-2, composed of two steel plates with identical dimensions but different yield strengths, were used during the tests. More specifically, the TSD-1 used Q235 steel, indicating a nominal yield strength of 235 MPa, while the TSD-2 used Q160, corresponding to a nominal yield strength of 160 MPa.

To further verify the mechanical properties of the designed TSDs, a series of unidirectional quasi-static tests were conducted on the TSD-1 and TSD-2 specimens. Due to the lack of loading equipment for the TSDs with small yield strengths, a simplified loading device is designed, as schematically illustrated in Fig. 8(a), and shown in Fig. 8(b). A pallet used to place weights (lead brick, 4.85 kg per one) is linked to the top of triangular steel plate through steel wires combined with a pulley. A string potentiometer is used to measure the horizontal displacement of the TSD. Three TSD-1s and three TSD-2s specimens were randomly selected for the quasi-static tests. Fig. 9 shows the global lateral force-displacement relationships of TSD1 and TSD2. In each subfigure, three dotted lines represent the recorded results from the quasi-static tests. Then an equivalent bilinear force-displacement curve is determined based on the three recorded curves. Table 3 lists the equivalent yield strength, stiffness, and the geometrical parameters of the TSDs. Note

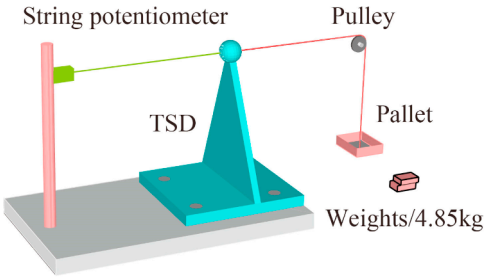

(a) Illustration for the load system

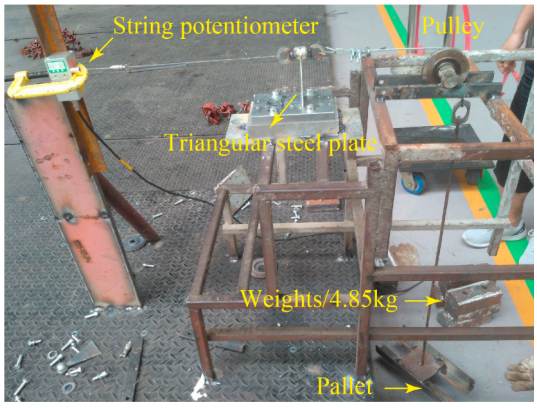

(b) Photo of the quasi-static test

Fig. 8. The quasi-static test for TSD.

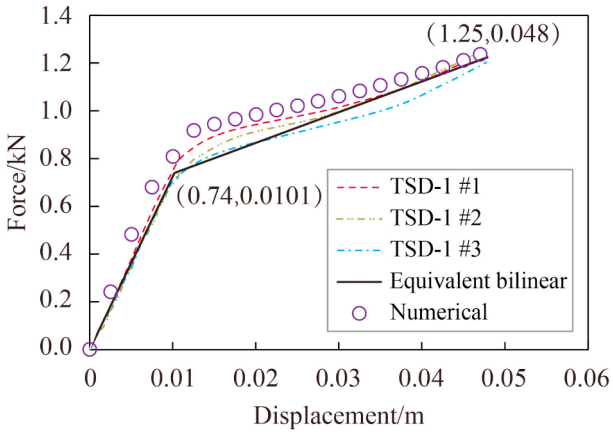

(a) TSD-1

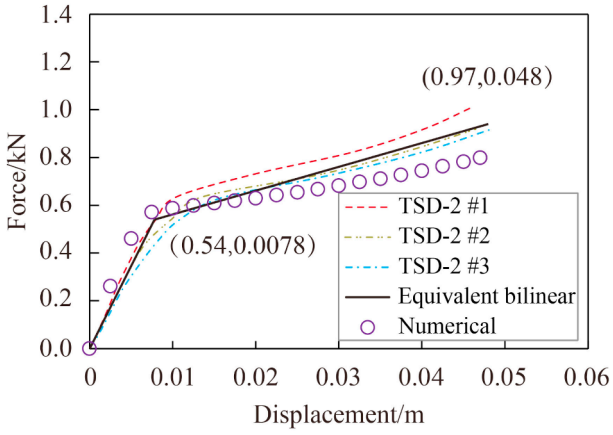

(b) TSD-2

Fig. 9. Force-displacement relationships of TSDs.

that the yield strength of TSDs used in the TSDSS1 and TSDSS2 is 0.74 and 0.54 kN, respectively. In addition, the predicted results using ABAQUS [32] are compared with equivalent bilinear results obtained from the experiments, which are shown in Fig. 9. Compared with the experimental results, the maximum discrepancies between the recorded and predicted results for TSD-1 and TSD-2 are 19% and 17%, respectively. In general, good agreements are achieved.

3. Test protocol

Table 4 lists the test case arrangements. White noise and four ground motions were selected as the earthquake excitations. The seismic excitation was only limited in the transverse direction and the Peak Ground Accelerations (PGAs) were scaled to 0.5 g except for the white noise (PGA = 0.1 g). Five test cases were performed for TSDSS1 and three test cases were performed for TSDSS2. After each ground motion except for the white-noise cases, intact TSDs were used to replace the tested ones. The TFS was excited by the same five ground motions sequentially.

Fig. 10 indicatively displays the adopted ground motions with PGA = 0.5 g and compressed time axis which was multiplied by a time scale-factor of 0.169. More specifically, the LCN260 contains a velocity pulse, while the other three do not (not shown for conciseness). The information of the adopted ground motions are: (1) LCN260, recorded in 1992 Landers earthquake (Lucerne Station, Magnitude, $M = 7.28$, Source distance, $R_{JB} = 2.19$ km, Average shear wave velocity at top 30 m of the site, $V_{s30} = 1369$ m/s); (2) Chi-Chi, recorded in 1999 Taiwan earthquake (TCU129 Station, $M = 7.62$, $R_{JB} = 1.83$ km, $V_{s30} = 511.18$ m/s); (3) El Centro, recorded in 1940 Imperial Valley earthquake (El Centro Station, $M = 6.95$, $R_{JB} = 6.09$ km, $V_{s30} = 213.44$ m/s) and (4) E10, a far-field and soft-site artificial wave, obtained from the report of probabilistic seismic hazard analysis for the site of the Sutong Bridge.

Fig. 11 presents the comparisons of acceleration response spectra with 3% damping ratio among the four time-compressed ground motions. They show significant differences on frequency contents. The E10 and El Centro ground motions contain more low-frequency contents, corresponding to predominant frequencies of 10 Hz and 11.1 Hz, respectively. By contrast, the Chi-Chi and LCN260 ground motions contain higher frequency contents, corresponding to predominant frequencies of 25 Hz and 50 Hz, respectively. Note that the E10 contains more low-frequency contents than all other three ground motions, thereby it should have significant influence on long period structures. It should be noted that the bridge systems were only excited transversally, test results hereinafter are just limited to the transverse direction of the bridge systems.

To illustrate the synchronicity and effectivity of the four shake-table system, corresponded acceleration spectra of the four recorded table motions by Tables A, B, C and D, together with the target motion of E10 (PGA = 0.5 g), are compared in Fig. 12(a); and the four recorded table displacement time-histories are also compared with target in Fig. 12(b). These results indicate that the four shake-table system can work synchronously as expected.

Table 3
Parameters of one TSD.

	Yield strength, kN	Equivalent stiffness, kN/m	Hardening ratio	Triangular steel plate				
				Height, cm	Width, cm	Thickness, cm	Material	Number of plate
TSD-1	0.74	73	0.185	11	7	0.3	Q235	2
TSD-2	0.54	69	0.155	11	7	0.3	Q160	2

Table 4
Testing case arrangements in transverse direction.

System	Case name	Motion name	PGA/g
TSDSS1 (With TSD-1s)	TSA-0	White noise	0.1
	TSA-1	Chi-Chi	0.5
	TSA-2	EL Centro	0.5
	TSA-3	E10	0.5
	TSA-4	LCN260	0.5
TSDSS2 (With TSD-2s)	TSB-0	White noise	0.1
	TSB-1	Chi-Chi	0.5
	TSB-2	E10	0.5
TFS (Without TSD)	TFC	White noise	0.1
		Chi-Chi	0.5
		LCN260	0.5
		El Centro	0.5
		E10	0.5

Note: PGA = peak ground acceleration.

4. Test results and discussion

4.1. Frequency and damping of the TSDSS and TFS

The first-order vibration mode of the test bridge is the lateral bending vibration of the deck at mid-span. In this regard, amplitude at the midpoint of the deck is quite large. Therefore, for the purpose of easy inspection, white-noise-induced responses at this point is selected for identifying the frequency and damping properties. Then it is transferred as Fourier spectra based on the Fast Fourier Transform (FFT) method [33]. The peak amplitudes in the Fourier spectra indicate the fundamental frequencies. The damping ratio of the system, ζ, is then evaluated by using the half-power bandwidth method that can be

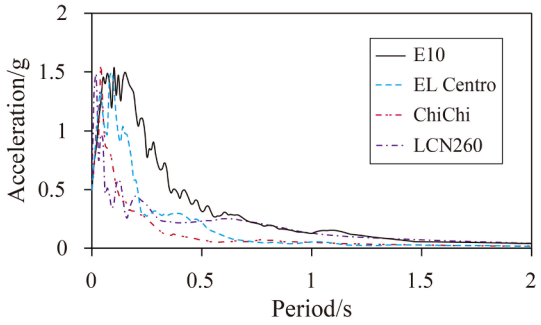

Fig. 11. Acceleration response spectra (3% damping ratio) of the time-compressed ground motions with PGA = 0.5 g.

expressed by Eq. (2):

$$\zeta = \frac{f_2 - f_1}{f_2 + f_1} \tag{2}$$

where f_1 and f_2 are frequencies at which the amplitudes equal $H_m/\sqrt{2}$ (H_m is the amplitude of Fourier spectrum).

Fig. 13 shows fundamental frequencies and damping ratios of the studied three systems (i.e., TSDSS1, TSDSS2 and TFS). For TFS, the damping ratio is 3.1% and the first frequency in the transverse direction is 0.61 Hz (i.e., period of 1.64 s). When this recorded model period is divided by the time scale-factor of 0.169, a period of 9.70 s is obtained, which is quite close to the results from numerical analysis of the Sutong Bridge reported by Wang et al. [25] and Ye et al. [34] (i.e., 10.0 s and 9.99 s, respectively). Such close results validate the design of the scale model. For TSDSS1 and TSDSS2, the approximately identical restraint

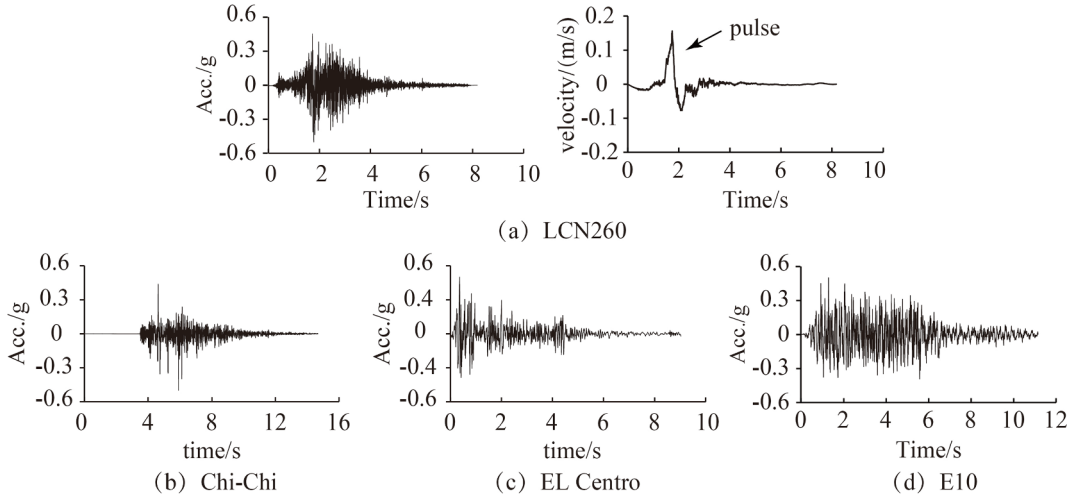

Fig. 10. Ground motions with a PGA of 0.5 g and compressed time axis.

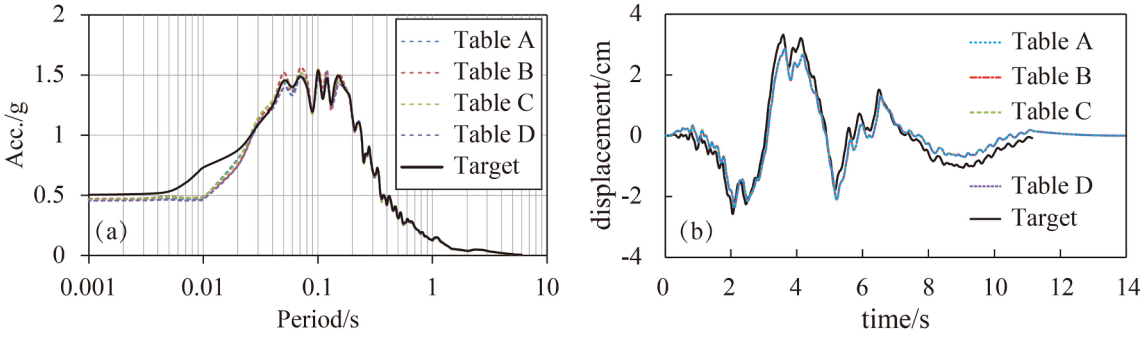

Fig. 12. Achieved table motions for the ground motion of Site E10: (a) acceleration spectra with 3% damping ratio, and (b) displacement time-histories.

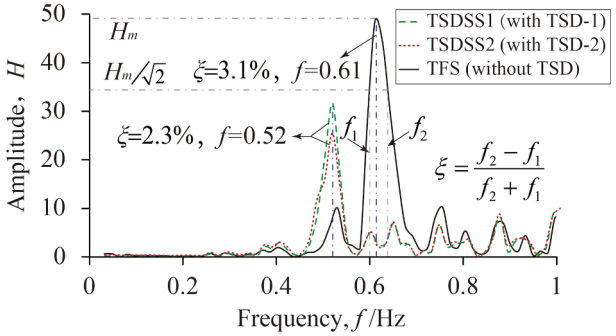

Fig. 13. Frequencies and damping ratios of different structural system.

stiffness to the deck provided by the deck-bent and deck-tower connections in the two systems results in the same first transversal frequency, both at 0.52 Hz (i.e., period of 1.92 s). The damping ratio is 2.3% for both TSDSSs. Compared with TFS, the period of TSDSS is elongated, as expected.

4.2. Transverse seismic force demands at deck-bent/tower connections

Fig. 14 presents comparisons for peak transverse horizontal forces at deck-bent and deck-tower connections between TFS and TSDSS1 under the four ground motions listed in Table 4. These horizontal forces are measured by tri-axial-force sensors placed at the base of TSDs and bearings, as shown in Fig. 5. More specifically, the horizontal forces transferred from the deck to the any bent consist of the shear force imposed to TSD and friction forces applied on SSSBs (sliding bearings).

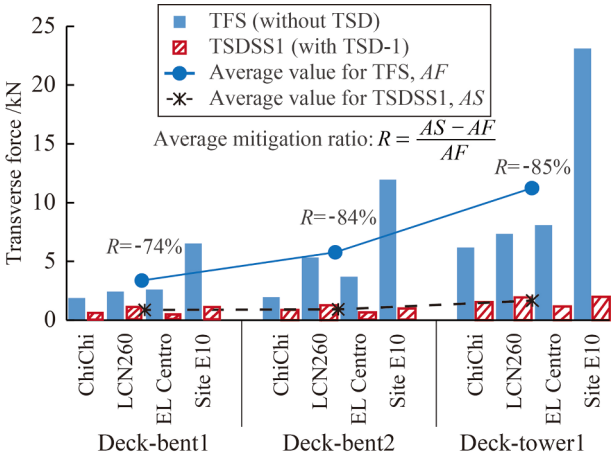

Fig. 14. Comparisons of peak transverse forces at deck-bent/tower connections between the TSDSS1 and TFS under different ground motions with PGA = 0.5 g.

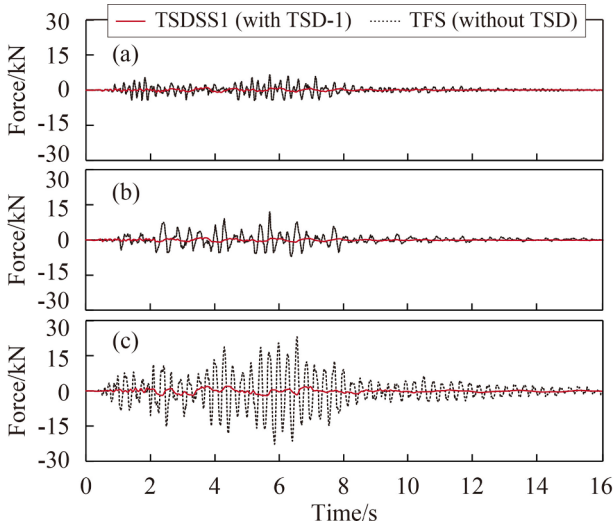

Fig. 15. Transverse force time-histories at the connections of different system under E10: (a) deck-Bent 1 connection, (b) deck-Bent 2 connection, and (c) deck-Tower 1 connection.

By contrast, the horizontal force transferred from the deck to the towers is merely the shear force carried by TSDs. In average, compared with the conventional TFS, the peak transverse force demands are reduced by 74%, 84% and 85% at the connections of deck-Bent 1, deck-Bent 2 and deck-Tower 1, respectively. More importantly, taking force demands at the deck-tower1 connection under the four ground motions as an example, slight variation of transverse forces from 1.17 to 1.98 kN was recorded in TSDSS, while in TFS, the force fluctuation, from 6.18 to 23.11 kN, was significant. Similar tendency can be observed in the deck-Bent 1 and deck-Bent 2 connections. This demonstrates that the sensitivity of TSDSS to ground motions is obviously lower than that of

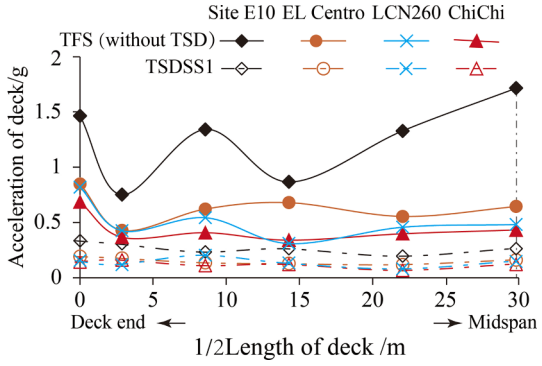

Fig. 16. Comparisons of peak transverse-acceleration along deck between the TSDSS1 and TFS under different ground motions with a PGA of 0.5 g.

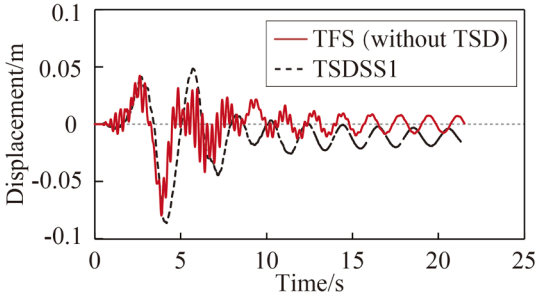

Fig. 17. Comparisons of displacement time-histories at deck-midpoint of different systems under 0.5 g E10.

the conventional TFS, which may be partially because the transverse forces transferred from deck to bents and towers are near the designed yield strength of TSDs. In addition, this result implies that the TSDSS is more favorable for bridges under unexpected large earthquakes.

Again from Fig. 14, for TFS it can be concluded that the forces transferred from the deck to bents and towers are apparently larger when the bridge model undergoes the E10 ground motion, because it contains more low-frequency contents than the other three ground motions as shown in Fig. 11.

Fig. 15 compares the force time-histories at deck-bent and deck-tower connections between TSDSS and TFS under E10. It is clear that the TSDSS can significantly reduce the forces transferred from deck to bents and towers compared with the TFS. Consequently, this will reduce the seismic demands at the substructures and towers.

4.3. Acceleration demands at the deck

Fig. 16 displays the peak transverse-acceleration along the deck of the TSDSS1 and TFS under the four ground motions. Due to the symmetry of structure, only left half of the whole-bridge results are presented. It is obvious that the peak transverse-acceleration of the deck in

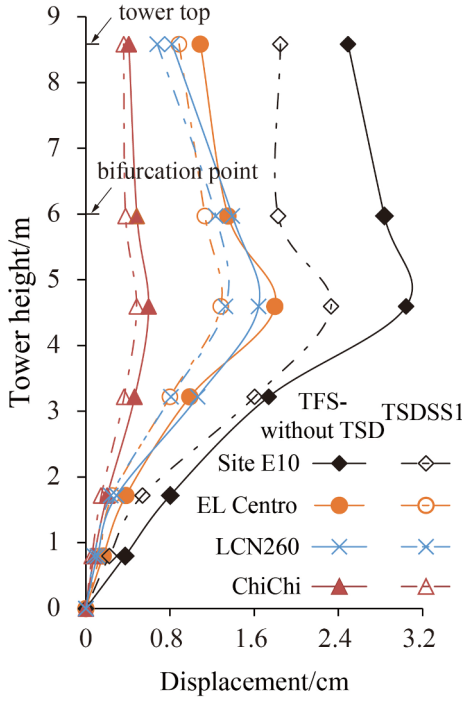

Fig. 18. Comparisons of peak transverse displacements along the tower shaft between the TSDSS1 and TFS under different ground motions with PGA = 0.5 g.

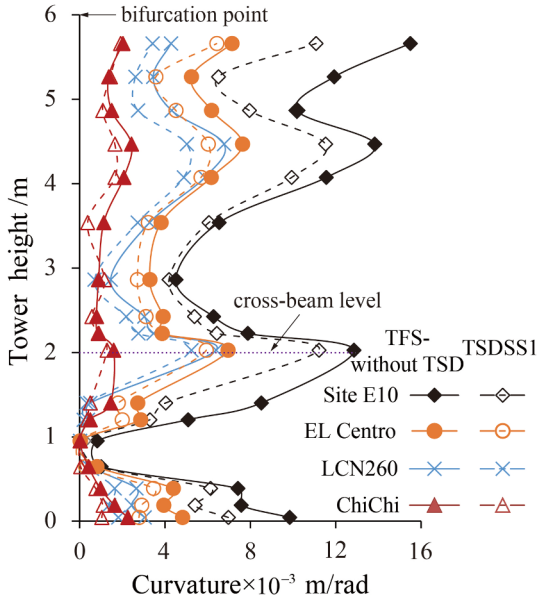

Fig. 19. Comparisons of peak curvatures along tower shaft between the TSDSS1 and TFS under different ground motions with a PGA of 0.5 g.

TSDSS is significantly lower than that of the TFS, which results in the remarkable decrease of the horizontal forces transferred from the deck to substructures and towers in the TSDSS as presented in Figs. 14 and 15. More importantly, the same conclusion can be addressed from Fig. 16, namely the sensitivity of the TSDSS to ground motions is obviously lower than that of the conventional TFS.

Fig. 17 depicts the displacement time-histories at the deck-midpoint of the TSDSS1 and TFS under E10. As can be seen from this graph, the oscillation with lower frequency in TSDSS1 is observed compared with the TFS. This is the reason why the peak transverse-acceleration at the deck of TSDSS is significantly lower than that of TFS.

4.4. Curvature and displacement demands at towers and bents

Fig. 18 illustrates the peak transverse displacements along tower shafts of TSDSS1 and TFS under the four ground motions. Compared with the TFS, smaller peak transverse displacements along the tower shaft of TSDSS are obtained. Moreover, for both of TSDSS and TFS, the maximum displacement of the inverted Y-shaped tower occurs at the tower-column regions below the bifurcation point under near- or far-fault ground motions; and the ground motion contain more low-frequency contents, such as the E10 ground motion in this study, triggers greater tower displacement demands.

Fig. 19 presents the curvature envelopes along the tower column of TSDSS1 and TFS under different ground motions. It can be concluded that TSDSS can reduce the section curvature along the tower column under near- and far-fault ground motions. Taking curvature demands at tower-bottom and pylon section above crossbeam as examples, compared with the conventional TFS, these peak curvature demands of TSDSS1 are averagely reduced by 41.7%, and 16.6%, respectively, under the four ground motions. Additionally, it is worth highlighting that the towers are more vulnerable when they experience earthquakes containing more low-frequency contents, such as the E10 ground motion in this study.

Fig. 20 depicts comparisons of section curvatures at Bent 2- and Tower1-bottom between the TSDSS and TFS under E10. Compared with the TFS, significant drop of the curvature demands at the tower and bent bottom sections is found in TSDSS. As can be seen from these results, the mitigation efficiency is more remarkable for bents because high-order modes of the tower should have significant contributions to its seismic responses [35].

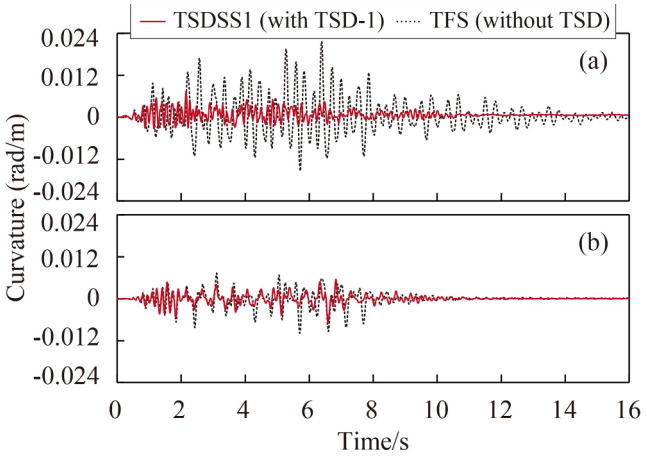

Fig. 20. Section curvature time-histories of different system under E10: (a) bottom section of bent2, and (b) bottom section of tower1.

According to aforementioned experimental results, it can be concluded that TSDSS is generally more robust than the conventional TFS for cable-stayed bridges against unexpected larger earthquakes.

4.5. Hysteretic properties and energy dissipation of TSD

To illustrate hysteretic properties of the TSD under different seismic excitations, hysteretic loops of the TSD-1 and one SSSB at connection of deck-Bent 2 under the four ground motions (PGA = 0.5 g) are all presented in Fig. 21. As can be seen from these graphs, the TSD possesses plump hysteretic loops under E10 and LCN260 ground motions, whereas maintains in elastic state under El Centro and Chi-Chi ground motions. This means that although the TSD is designed to have excellent energy dissipation capacity, the quantity of energy dissipation is related to ground motions. In particular, the pulse of velocity in LCN260 ground motion leads to less hysteretic cycles in the TSD

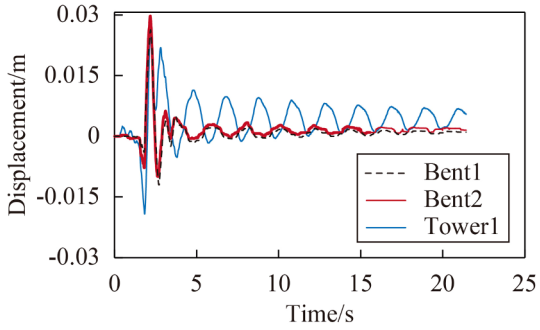

Fig. 22. Displacements at deck-bent/tower connections of the TSDSS1 under LCN260 with velocity pulse.

(Fig. 21(c)). It should be highlighted that the TSDSS has a remarkable seismic performance regardless of whether the TSDs yield or not, as discussed in the previous sections. Compared with the TSD, the SSSB presents relatively narrow hysteretic loops (approximately rectangular, as expected) and its capacity of energy dissipation mainly depends on the normal force at the bearing.

Fig. 22 typically plots the relative displacement time-histories of TSD at the connections of deck-Bent 1, deck-Bent 2 and deck-Tower 1 in the TSDSS1 under LCN260 with PGA = 0.5 g. Note that the pulse of velocity in the LCN260 ground motion triggers the displacement pulse at the TSDs (or deck).

To further reveal the property of energy dissipation of the TSDSS, Fig. 23 shows the cumulative energy time-history absorbed by TSDs and SSSBs in the TSDSS1 under the E10 and LCN260 ground motions, as indicative examples. For the case of 0.5 g E10, as shown in Fig. 23(a), the energy dissipated by all the TSDs is 0.610 kJ, while the energy dissipated by all the SSSBs is 0.271 kJ, which indicates that the TSD has a more excellent energy dissipation capacity. The same conclusion can be obtained for LCN260 ground motion from Fig. 23(b). Additionally, a comparison for energy dissipation quantity of TSDSS1 under the two

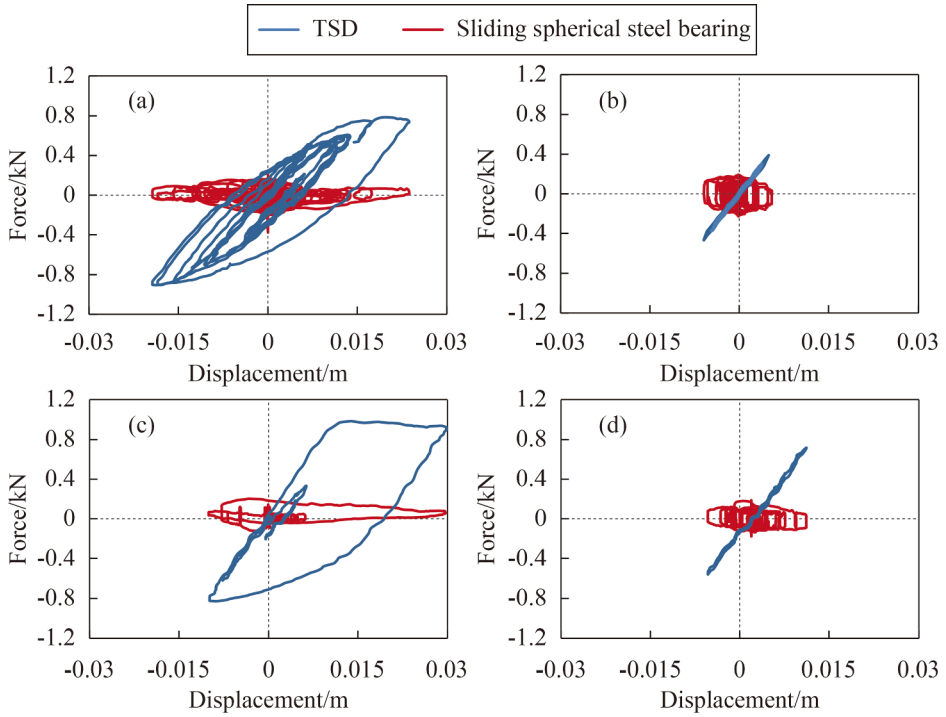

Fig. 21. Hysteretic cycles of TSD and SSSB at deck-bent2 connection under different ground motions: (a) E10, (b) El Centro, (c) LCN260, and (d) Chi-Chi.

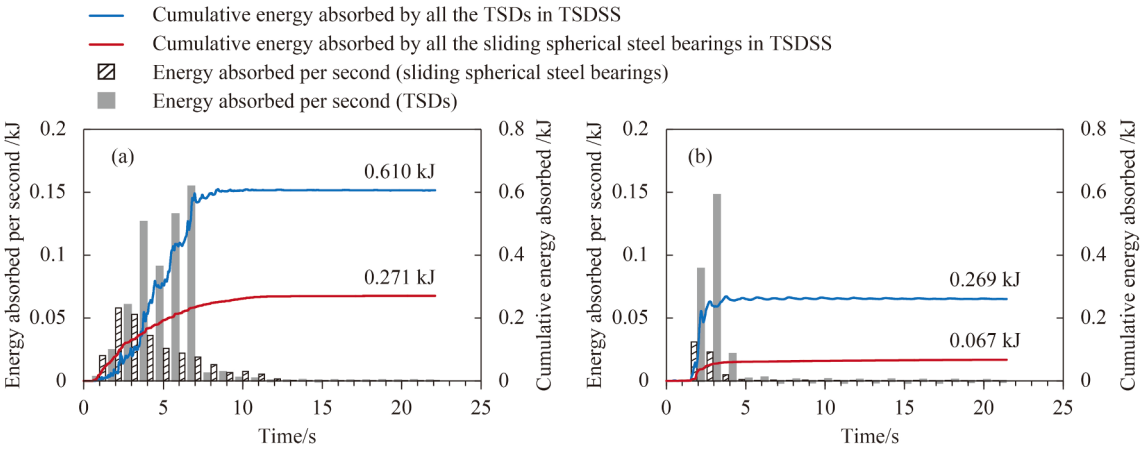

Fig. 23. Energy dissipation of the TSDSS under different ground motions: (a) E10, and (b) LCN260.

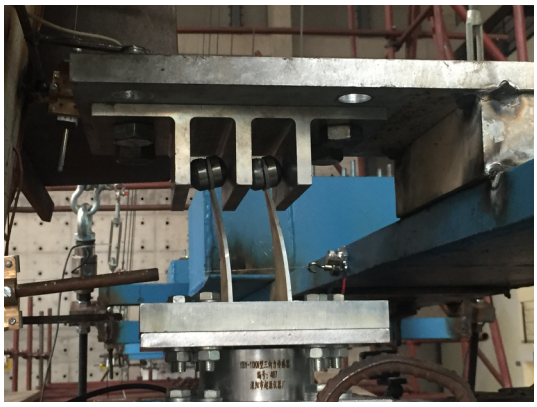

Fig. 24. The photo of TSD at deck-tower1 connection after the action of E10.

ground motions show that the total energy dissipated by all TSDs and SSSBs under E10 is 2.62 times that under LCN260 (0.881 kJ and 0.336 kJ for E10 and LCN260, respectively), which indicates that the quantity of energy dissipated by isolation devices are related to ground motions. This issue may be worth concerned in future studies. Furthermore, the velocity pulse of LCN260 obviously triggers a transient energy dissipation as observed at 2–3 s in Fig. 23(b). This is because the dissipated energy is mainly cumulated at the large cycle that is triggered by the pulse.

Fig. 24 shows the photo of TSD at deck-Tower 1 connection in TSDSS1 after the excitation of E10 ground motion. A slight residual deformation was observed since the TSD experienced plastic deformation under this ground motion. Except for that, no damages or failure are observed in the TSDs at all the test cases. Additionally, load paths from the deck to bents and towers are never interrupted during the tests. This also validates that the configuration of TSD can accommodate the complex load transmission path under dynamic loads.

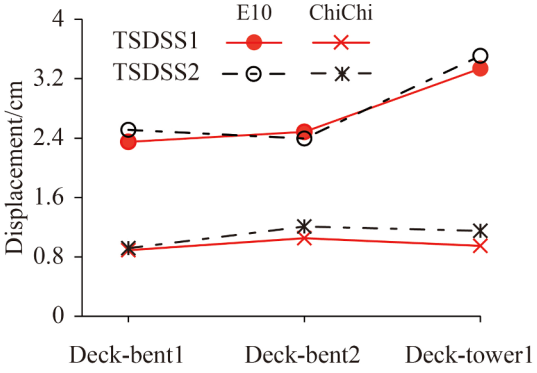

Fig. 25. The impact of TSD yield strength on the peak displacements at deck-bent/tower connections.

4.6. Impact of TSD yield strength on seismic behaviors of the TSDSS

The impact of TSD yield strength on the seismic behavior of TSDSS for cable-stayed bridges is discussed here according to experimental results. Seismic demands of TSDSS1 and TSDSS2 under soft- and stiff-site ground motions (E10 and Chi-Chi ground motions, respectively), are compared. As aforementioned, the yield strength of TSDs used in TSDSS1 is 0.74 kN (TSD-1), while that used in TSDSS2 is 0.54 kN (TSD-2).

Fig. 25 shows the impact of the TSD yield strength on the displacement demands at deck-bent and deck-tower connections. In general, the peak displacements at deck-bent and deck-tower connections can be decreased by increasing the yield strengths of TSDs.

Fig. 26 indicatively shows hysteretic loops of TSD-1 and TSD-2 installed at the deck-Tower 1 connection. As presented in this graph, both TSDs possess plump hysteresis loops under E10 ground motion. As expected, the peak displacements of TSD-1 are relatively smaller because of its higher yield strength than TSD-2. Meanwhile, the peak forces of TSD-1 are larger than TSD-2.

Fig. 27 shows the impact of TSD yield strength on force demands at deck-bent/tower connections and curvature demands at bent-bottom and tower column sections. According to these experiment results, increasing the yield strength of TSD leads to larger peak horizontal forces

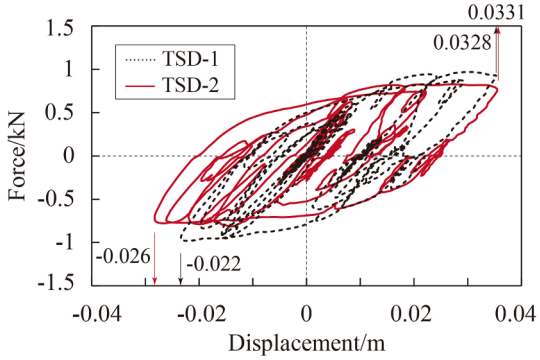

Fig. 26. The hysteretic loops of TSD with different yield strength (E10).

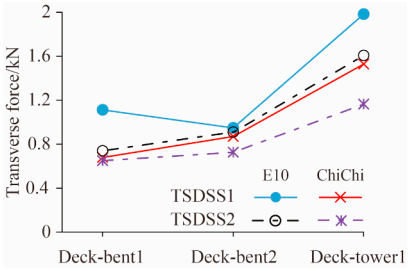

(a) Comparisons of transverse forces at deck-bent and tower connections

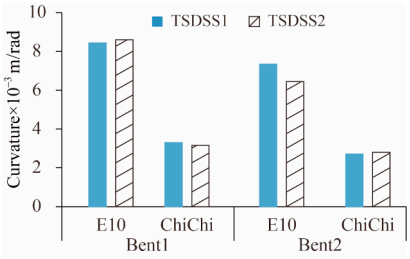

(b) Comparisons of the curvature at bottom section of bents

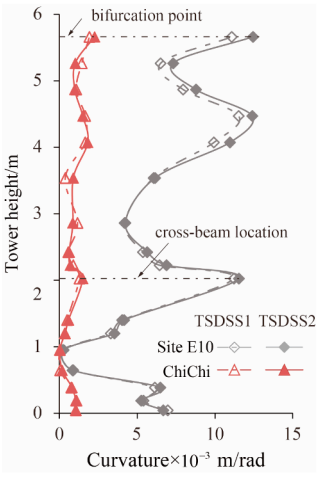

(c) Comparisons of the curvature along tower column

Fig. 27. The impact of TSD yield strength on seismic response of structure.

transferred from the deck to bents and towers. As illustrated in Fig. 27(b) and (c), the small difference of TSD yield strengths (0.74 kN for TSD-1 versus 0.54 kN for TSD-2) may not trigger significant influence on curvatures at bents and towers.

With regard to the impact of site types of ground motions, section curvatures at bent-bottom and tower column under the soft-site ground motion (E10) are obviously greater than that under the stiff-site one (Chi-Chi), because the soft-site ground motion contains more low-frequency contents as previously shown in Fig. 11.

5. Numerical modeling and validation

To assist engineers to efficiently predict the seismic performance of cable-stayed bridges, a reliable and simple numerical model is a desirable practice solution. To this end, a finite element model representing the shake-table test is built in *OpenSees* [28] and validated using the recorded results. Considering the length of the article, one typical TSDSS test case (i.e., TSA-3 as shown in Table 4) is selected, in which the TSD-1 is adopted and E10 ground motion is selected as seismic excitation. Since the towers in this case generally remain elastic as expected, elastic beam-column elements are used to model the bents, towers and deck for simplicity. In addition, it is worth noting that the scaled test model, rather than the corresponding prototype, is simulated in this paper, because some simplification procedures (e.g., reducing and reforming the cables) had been used when preparing the shake-table test, which inevitably raise the difficulty for the model-prototype transformation merely based on the similarity coefficients.

5.1. Modeling description

As illustrated in Fig. 28, a three-dimensional finite element model of the 1/35-scale model-bridge equipped with TSDs is established in *OpenSees* [28]. The floating deck system is used in the longitudinal direction. For the elastic beam-column elements that model the bents, towers and deck, geometric properties of the sections (i.e., areas and inertia of gross) are determined based on their geometric configurations shown in Fig. 2. The measured Young's modulus of concrete is 10348 MPa. The *Pdelta transformation* command in *OpenSees* is used to account for the P-Δ effect [36,37]. Cables are simulated using truss elements accounting for sag effects using the Ernst method (modified elasticity modulus of cables) [38]. The Young's modulus of the cable material is 195 GPa. To simulate pre-tension forces in cables, initial strains are assigned to the truss elements. All the bents and towers are fixed at their bottoms because the soil–structure interaction is neglected in the shake table test.

TSDs at the deck-bent/tower connections are simulated by zero-length elements with the Steel01 material, as schematically shown in Fig. 28. The yield strength, initial elastic stiffness and hardening ratio of one TSD are 0.74 kN, 73 kN/m and 0.185, respectively. On the other hand, SSSBs at the deck-bent connections are simulated by zero-length elements with the elastic-perfectly plastic material. For each SSSB, the yield force is calculated by multiplying the normal force by the friction coefficient (set as 0.02), as mentioned in Section 2.4. The initial stiffness of the SSSB model is equal to the yield force divided by 0.002 m as recommended in [1].

Since the four shake tables work synchronically, as discussed in Section 3, the recorded motion by Table B is used as seismic input for the numerical model. In the dynamic analysis, Newton with Line Search algorithm [39] and β-Newmark integrator with parameters $\beta = 0.25$ and $\gamma = 0.5$ are used to solve the matrix equations. The convergence tolerance is set to 1.0×10^{-5}. Note that the gravity analysis is conducted before performing the dynamic analyses.

5.2. Comparisons of test and numerical results

Fig. 29 presents comparisons of TSD deformations (or relative displacements) at different connections between the predicted and recorded results. As can be seen from these figures, the predicted results are almost identical to the test data, which indicates that the established finite element model can accurately estimate the deformations of TSDs under earthquakes.

Fig. 30 compares predicted and recorded displacement results at the tower-top and bifurcation point. It is seen that the finite element model can generally capture the peak responses although some discrepancies in part of the time histories are observed. These discrepancies may be attributed to the simplified modelling technique for the tower (i.e., elastic beam-column element), which cannot perfectly reflect the minor cracks in the tower during shaking. Nevertheless, considering the merits of modelling simplicity and computational efficiency, it is reasonable to conclude that the established finite element model is capable of capturing the seismic responses of cable-stayed bridges equipped with TSDs.

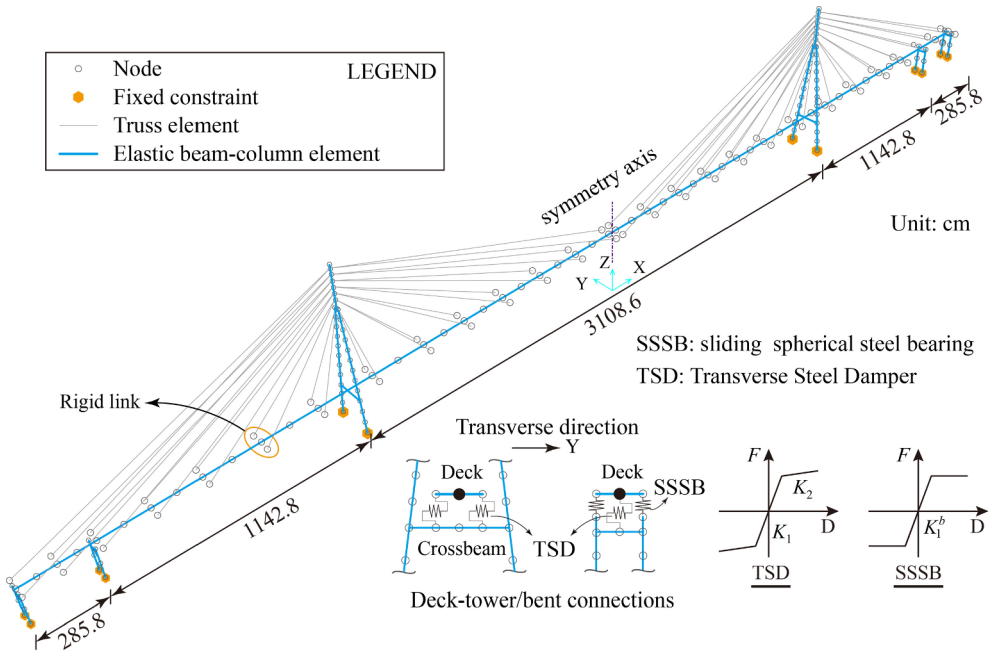

Fig. 28. Schematic illustration for the numerical model of the test bridge with TSDs.

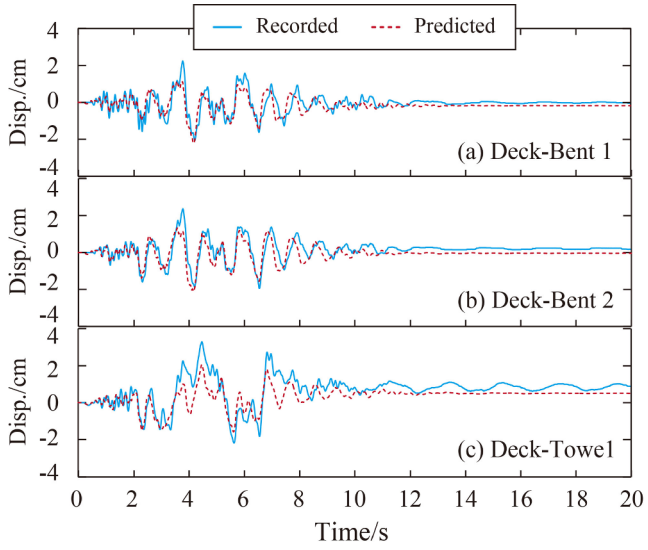

Fig. 29. Comparisons of TSD deformation time-histories at different connections between predicted and recorded results under E10.

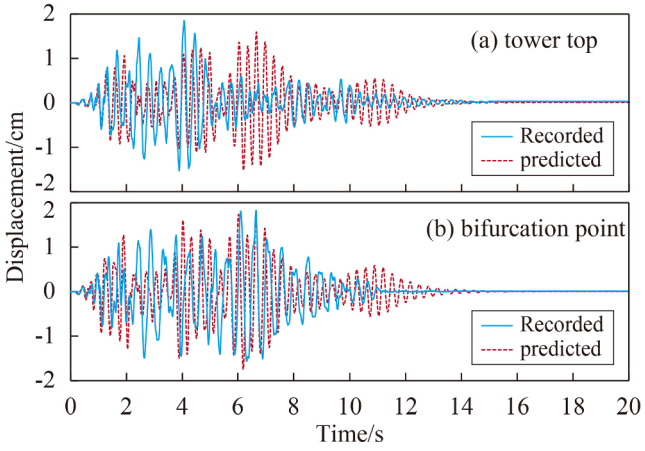

Fig. 30. Comparisons of tower displacement demands between predicted and recorded results under E10.

6. Conclusions

The objective of this study is to experimentally investigate the seismic behaviors of TSDSS for long span cable-stayed bridges and to verify the reliability and mitigation efficiency of TSDSS under near- and far-fault ground motions. For this purpose, a series of tests on a 1/35-scale model of Sutong Bridge were conducted using a four-shake-table testing system. During the study, the seismic behaviors of TSDSS and TFS, and the impact of TSD yield strength on the seismic behaviors of TSDSS were assessed. Furthermore, a numerical model of the tested bridge was set up and validated. The main remarkable findings and conclusions are drawn as follows:

(1) Compared with the TFS, TSDSS can significantly reduce transverse force demands at deck-bent and deck-tower connections, and decrease lateral displacement and curvature demands along tower shafts. It can also significantly reduce curvature demands at the bottom section of bents, meanwhile limiting relative displacements at deck-bent and deck-tower connections to an acceptable level for practice.
(2) The sensitivity of TSDSS to ground motions is obviously lower than that of the conventional TFS, indicating a generally robust behavior for TSDSS under earthquakes.
(3) The hysteretic behavior of TSD is related to the characteristics of ground motions. Especially, the pulse of velocity in a ground motion triggers the displacement pulse at the TSDs. Nevertheless, TSDSS presents reliable and excellent seismic performance, regardless of near- or far-field ground motions.
(4) Increasing the yield strength of TSDs can reduce relative displacement demands at deck-bent and deck-tower connections.
(5) The validated numerical model is capable of predicting the seismic responses of cable-stayed bridges equipped with TSDs.

Acknowledgments

This work is supported by the National Basic Research Program of China (No. 2013CB036302). All staffs in the Multi-Functional Shaking

Table Lab of Tongji University are greatly acknowledged, especially Drs. Jianzhong Li, Yan Xu, Zhongguo Guan and Chengyu Yang who provided lots of insightful suggestions to the test. Special thanks to Mr. Tengfei Liu for providing comments to improve the manuscript. The authors also acknowledge the anonymous reviewers who have contributed to essentially improving the paper.

References

[1] Ministry of Housing and Urban Rural Development of P. R. Code for seismic design of urban bridges (CJJ 166-2011). Beijing,China: China Architecture & Building Press; 2011.
[2] Ministry of Communications of the People's Republic of China.Guidelines for seismic design of highway bridges. Beijing, China: People's communication press; 2008.
[3] Chang KC, Mo YL, Chen CC, Lai LC, Chou CC. Lessons learned from the damaged Chi-Lu cable-stayed bridge. J Bridg Eng 2004;9:343–52. https://doi.org/10.1061/(ASCE)1084-0702(2004) 9:4(343).
[4] Ye A, Hu S, Fan L. Seismic displacement control for super-long-span cable-stayed bridges. China Civ Eng J 2004;37(12):38–43. [in Chinese].
[5] Soneji BB, Jangid RS. Passive hybrid systems for earthquake protection of cable-stayed bridge. Eng Struct 2007;29:57–70. https://doi.org/10.1016/j.engstruct.2006.03.034.
[6] Valdebenito GE ÁCA. Seismic protection of cable-stayed bridges applying fluid viscous dampers. Barcelona: Centre Internacional de Mètodes Numèrics en Enginyeria (CIMNE); 2009.
[7] Martínez-Rodrigo MD, Filiatrault A. A case study on the application of passive control and seismic isolation techniques to cable-stayed bridges: A comparative investigation through non-linear dynamic analyses. Eng Struct 2015;99:232–52. https://doi.org/10.1016/j.engstruct.2015.04.048.
[8] Calvi GM, Sullivan TJ, Villani A. Conceptual seismic design of cable-stayed bridges. J Earthq Eng 2010;14:1139–71. https://doi.org/10.1080/13632469.2010.505275.
[9] Ye A, Fan L. Seismic response reduction of a super-long-span cable-stayed bridge by adding dampers. J Tongji Univ 2006;34(7):859–63. [in Chinese].
[10] Yan B, Du XL, Han Q. Application of hybrid seismic mitigation and isolation device to seismic design of single-pylon cable-stayed bridge. Bridg Const 2014;44(6):101–6. [in Chinese].
[11] Shen X, Camara A, Ye A. Effects of seismic devices on transverse responses of piers in the Sutong Bridge. Earthq Eng Eng Vib 2015;14:611–23. https://doi.org/10.1007/s11803-015-0049-7.
[12] Shen X, Wang X, Ye Q, Ye A. Seismic performance of transverse steel damper seismic system for long span bridges. Eng Struct 2017;141:14–28. https://doi.org/10.1016/j.engstruct.2017.03.014.
[13] Camara A, Cristantielli R, Astiz MA, Málaga-Chuquitaype C. Design of hysteretic dampers with optimal ductility for the transverse seismic control of cable-stayed bridges. Earthq Eng Struct Dyn 2017;46:1811–33. https://doi.org/10.1002/eqe.2884.
[14] Infanti S, Papanikolas P, Benzoni G, Castellano MG. Rion-antirion bridge: design and full-scale testing of the seismic protection devices. In: Proc. 13th World Conf. Earthq. Eng.; 2004.
[15] Ismail M, Casas JR, Rodellar J. Near-fault isolation of cable-stayed bridges using RNC isolator. Eng Struct 2013;56:327–42. https://doi.org/10.1016/j.engstruct.2013.04.007.
[16] Guan Z, You H, Li J. Lateral isolation system of a long-span cable-stayed bridge with heavyweight concrete girder in a high seismic region. J Bridg Eng 2017;22:04016104. https://doi.org/10.1061/(ASCE)BE.1943-5592.0000965.
[17] Abdel Raheem SE, Hayashikawa T. Energy dissipation system for earthquake protection of cable-stayed bridge towers. Earthq Struct 2013;5:657–78. https://doi.org/10.12989/eas.2013.5.6.657.
[18] Yang CY, Cheung MMS. Shake table test of cable-stayed bridge subjected to non-uniform excitation. Proc Eng 2011;14:931–8. https://doi.org/10.1016/j.proeng.2011.07.117.
[19] Zhou R, Zong Z, Huang X, Xia Z. Seismic response study on a multi-span cable-stayed bridge scale model under multi-support excitations. Part II: numerical analysis. J Zhejiang Univ Sci A 2014;15:405–18. https://doi.org/10.1631/jzus.A1300340.
[20] Liang F, Jia Y, Sun L, Xie W, Chen H. Seismic response of pile groups supporting long-span cable-stayed bridge subjected to multi-support excitations. Soil Dyn Earthq Eng 2017;101:182–203. https://doi.org/10.1016/j.soildyn.2017.07.019.
[21] Wang R, Xu Y, Li J. Transverse seismic behavior studies of a medium span cable-stayed bridge model with two concrete towers. J Earthq Eng 2017;21:151–68. https://doi.org/10.1080/13632469.2015.1118710.
[22] Yi J, Li J. Longitudinal seismic behavior of a single-tower cable-stayed bridge subjected to near-field earthquakes. Shock Vib 2017.;2017. https://doi.org/10.1155/2017/1675982.
[23] Xu Y, Wang R, Li J. Experimental verification of a cable-stayed bridge model using passive energy dissipation devices. J Bridg Eng 2016;21:04016092. https://doi.org/10.1061/(ASCE)BE.1943-5592.0000966.
[24] Jiang YI, Sun PJL. Shaking table tests for transverse aseismic control of cable-stayed bridges. J Vib Shock 2018;37(3):47–53. [in Chinese].
[25] Wang H, Hu R, Xie J, Tong T, Li A. Comparative study on buffeting performance of Sutong Bridge based on design and measured spectrum. J Bridg Eng 2013;18:587–600. https://doi.org/10.1061/(ASCE)BE.1943-5592.0000394.
[26] Moncarz PD, Krawinkler H. Theory and application of experimental model analysis in earthquake engineering. Rep - Stanford Univ John A Blume Earthq Eng Cent; 1981.
[27] Coutinho CP, Baptista AJ, Dias Rodrigues J. Reduced scale models based on similitude theory: a review up to 2015. Eng Struct 2016;119:81–94. https://doi.org/10.1016/j.engstruct.2016.04.016.
[28] McKenna F. OpenSees: A framework for earthquake engineering simulation. Comput Sci Eng 2011;13:58–66. https://doi.org/10.1109/MCSE.2011.66.
[29] Wei B, Wang P, Liu W, Yang M, Jiang L. The impact of the concave distribution of rolling friction coefficient on the seismic isolation performance of a spring-rolling system. Int J Non Linear Mech 2016;83:65–77. https://doi.org/10.1016/j.ijnonlinmec.2016.04.001.
[30] Yang H, Liu S, Yuan W. Experiment based seismic behavior investigation of a sliding controlled isolation system. J Perform Constr Facil 2017;31:04016106. https://doi.org/10.1061/(ASCE)CF.1943-5509.0000963.
[31] Wei B, Zuo C, He X, Jiang L. Numerical investigation on scaling a pure friction isolation system for civil structures in shaking table model tests. Int J Non Linear Mech 2018;98:1–12. https://doi.org/10.1016/j.ijnonlinmec.2017.09.005.
[32] Liu T, Shen X, Ye A. Hysteretic model parameter of the steel triangular plate damper in bridges. Structural Eng 2014;30(6):54–60. [in Chinese].
[33] Cooley JW, Lewis PAW, Welch PD. The fast fourier transform and its applications. IEEE Trans Educ 1969;12:27–34. https://doi.org/10.1109/TE.1969.4320436.
[34] Ye ASZ. effect of cable vibration on seismic response of super long span cable-stayed bridges. J Tongji Univ (Natural Sci) 2010;38(2):158–63. [in Chinese].
[35] Camara A, Astiz MA. Analysis and control of cable-stayed bridges subject to seismic action. Struct Eng Int J Int Assoc Bridg Struct Eng 2014;24:27–36. https://doi.org/10.2749/101686614X13830790993762.
[36] MacRae GA. P-Δ effects on single-degree-of-freedom structures in earthquakes. Earthq Spectra 1994;10(3):539–68.
[37] Wang X, Shafieezadeh A, Ye A. Optimal intensity measures for probabilistic seismic demand modeling of extended pile-shaft-supported bridges in liquefied and laterally spreading ground. Bull Earthq Eng 2018;16:229–57. https://doi.org/10.1007/s10518-017-0199-2.
[38] Karoumi R. Some modeling aspects in the nonlinear finite element analysis of cable supported bridges. Comput Struct 1999;71:397–412. https://doi.org/10.1016/S0045-7949(98)00244-2.
[39] Crisfield MA. Nonlinear finite element analysis of solids and structures, Volume 1: essentials. Wiley; 1991.